ORIGINAL PAPER

A Straightforward Immunoassay Applicable to a Wide Range of Antibodies Based on Surface Enhanced Fluorescence

Ruohu Zhang · Zhuyuan Wang · Chunyuan Song · Jing Yang · Yiping Cui

Abstract A straightforward immunoassay based on surface enhanced fluorescence (SEF) has been demonstrated using a fluorescent immune substrate and antibody functionalized-silver nanoparticles. Unlike the conventional SEF-based immunoassay, which usually uses the dye-labeled antibodies and the metallic nanostructured-substrates, the presented immune system does not need the antibodies to be labeled with dye molecules. Thus, this immunoassay can be easily applied to the detection of a wide range of target antigens, which is of great importance for its practical application. The experimental results show that this immunoassay has a good specificity as well as the capacity of quantitative detection. Basically, the surface density of the immuno-adsorbed silver nanoparticles increases with the increased amount of target antigens, resulting in a fluorescence enhancement up to around 7 fold. The dose-responsive performance of the immunoassay has been investigated and the limit of detection (LOD) is 1 ng/mL. Due to its simple preparation method and the wide range of detectable antigens, this presented immunoassay is expected to be helpful for extending the SEF-based application.

Keywords Surface enhanced fluorescence · Surface plasmon resonance · Immunoassay · Ag nanoparticle · Substrate

Introduction

In recent years, fluorescence has been established to be a powerful tool in medical diagnostics and biotechnology.

R. Zhang · Z. Wang · C. Song · J. Yang · Y. Cui (✉)
Advanced Photonics Center, Southeast University,
Nanjing 210096, People's Republic of China
e-mail: cyp@seu.edu.cn

Employing fluorescence to detect biomolecules, e.g., fluorescence immunoassay, has been widely used [1]. Recently, surface enhanced fluorescence (SEF), or metal enhanced fluorescence (MEF) has emerged, which might exhibit some advantages compared with the conventional fluorescence technique [2–5]. When a fluorescent molecule is placed in proximity to a metallic nanostructure, a significantly enhanced fluorescence emission may be obtained, accompanied by a decreased lifetime and an increased photostability. This phenomenon represents an important aspect of metal–molecule interactions [2, 3]. The earliest theoretical studies on the SEF effect date back to the 1980s [6–8], and it is commonly believed that several processes are involved, including an enhanced excitation near field, an increased radiative decay rate of the molecule, and an enhanced out-coupling efficiency of the fluorescence emission transferred from the molecule to the metallic nanostructure, as described by the radiating plasmon model (RPM) raised by Lakowicz [9]. Recently, experimental evidences have also been reported to address this issue [10].

During the past decade, a number of SEF-based immunoassays have been reported. Different metallic nanostructures, either chemical grown [11], vapor deposited [12], or electrochemically prepared [13], were used as the SEF substrate. Matveeva et al. developed a highly efficient SEF substrate, with silver nanoparticles on an underlying metal film, in which over 50-fold signal enhancement was obtained [14]. Nooney et al. introduced a homogeneous silver nanoparticle substrate for fluorescence immunoassays, and significant improvements in the limit of detection were obtained as 0.086 ng/mL [15]. Recently, a novel gap-plasmon-tunable silver bilayer nanoparticle film was also developed by us, and its ability in SEF-based immunoassay was demonstrated [16]. In all the above reports, the SEF-based immunoassays consist of two separate components. One is the SEF substrate, which is the focus of the design.

The other is the immunoassay component, which is the same as that in the traditional fluorescence immunoassay scheme.

In such SEF-based immunoassay schemes, a fluorescently labeled antibody has been used to specifically detect the target antigen. The fluorescent labeling technique has made a great success ever since its introduction in the 1940s [17]. However, relatively complex and expensive procedures are needed for the labeling. The effect of the labeling on the functionality of the antibody also has to be evaluated [18]. Moreover, the metallic nanostructure surface is different from the traditional protein reactive surface in both chemical composition and surface morphology, and hence the immobilization of proteins on the SEF substrates needs further investigation. Moreover, the inhomogeneity of the SEF substrates has been considered as one possible reason for the lack of the analytical performance in most SEF-based immunoassays [15].

Herein, a novel SEF-based immunoassay scheme applicable to a wide range of antibodies is demonstrated, wherein the uses of the dye-labeled antibodies and the metallic nanostructures are avoided. A fluorescent immune substrate has been constructed and used for antigen immobilization, which is expected to provide a more homogeneous surface than the metallic nanostructure substrates, and thus an analytical performance with a better reproducibility. The silver-antibody nanoconjugate (SANC) has been synthesized and used for the specific recognition of the surface-bound antigens. The overall immunoassay structure is shown in Scheme 1. Upon the specific adsorption of the SANC onto the substrate, an enhancement of the fluorescence can be observed. Varying antigen concentration is observed to result in varying fluorescence enhancement factors, and a limit of detection (LOD) of
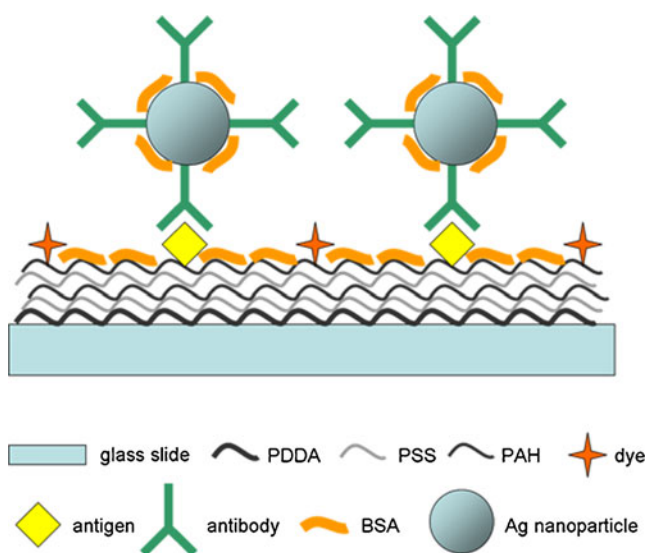
1 ng/mL has been determined using our immunoassay scheme. Therefore, the applicability of our SEF-based immunoassay is demonstrated, avoiding the inconvenience in the uses of both the dye-labeled antibodies and the metallic nanostructure substrates. The present work is expected to provide new insights into the SEF-based applications.

Experimental Section

Materials

Poly (diallyldimethylammonium chloride) (PDDA), MW 100,000–200,000, Poly (sodium styrenesulfonate) (PSS), MW 70,000, poly (allylamide hydrochloride) (PAH), MW 15,000, 1-ethyl-3-(3-dimethylaminopropyl) carbodiimide (EDC) and N-hydroxysuccinimide (NHS) were purchased from Sigma-Aldrich. Glutaraldehyde was purchased from Alfa Aesar. Silver nitrate was purchased from Shanghai Shenbo Chemical Co., Ltd. Trisodium citrate dihydrate was purchased from Jiangsu Qiangsheng Chemical Co., Ltd. Rose Bengal (RB) was purchased from Shanghai Jingchun Chemical Co., Ltd. Sodium tetraborate (Na$_2$B$_4$O$_7$) was purchased from Nanjing Chemical Co., Ltd. Human Immunoglobulin G (hIgG), goat anti-human immunoglobulin G (GAH IgG) and bovine serum albumin (BSA) were purchased from Beijing Bioss Biotech Co., Ltd. Polyoxyethylene (20) sorbitan monolaurate (Tween-20) and Tris (hydroxymethyl) aminomethane (TRIS) were purchased from Sinopharm Chemical Reagent Co., Ltd. TBS buffer solution was prepared by dissolving NaCl (8.76 g) and TRIS (1.21 g) in water (500 mL). TBS-T buffer solution was prepared by mixing Tween-20 (0.25 g) with TBS (500 mL). BBS solution was prepared by dissolving sodium tetraborate in water to a concentration of 2 mM, reaching a pH of 9.0. The water used throughout the experiments was ultrapure deionized water.

Synthesis of Ag Nanoparticles

Colloidal Ag nanoparticles were synthesized according to Lee's method [19]. Briefly, an aqueous solution of AgNO$_3$ (0.0849 g, 1 mM) was brought to boiling under stirring. Trisodium citrate solution (10 mL, 1 % w/w) was then added. The mixture was boiled for 1 h under vigorous stirring and then allowed to cool slowly to room temperature. The as-prepared Ag nanoparticles were greenish yellow in color and characterized by an extinction peak at 416 nm.

Synthesis of the SANC

The SANC were synthesized according to previously reported methods with some modifications [20–22]. The

Scheme 1 The structure of the presented SEF-based immunoassay applicable to a wide range of antibodies

Ag nanoparticles (1 mL) were purified by centrifugation and redispersed in BBS solution (1 mL), to which a proper volume of K_2CO_3 solution (0.2 M) was added and the pH of the mixture was adjusted to 9.0. The GAH IgG (70 μL, 1 mg/mL in BBS) was then added and the mixture was incubated at 37 °C for 1 h, during which the antibodies adsorbed onto the Ag nanoparticles through a combination of ionic and hydrophobic interactions. After a BSA solution (24 μL, 5 % in BBS) was added and then incubated for another 0.5 h, the mixture was purified by centrifugation and redispersed in BBS solution (200 μL).

Preparation of the Fluorescent Immune Substrate

The glass slides were first treated with a 4:1 (v/v) mixture of H_2SO_4 (98 %) and H_2O_2 (30 %) under sonication for 4 h to remove the impurities and to activate the surface. After thoroughly rinsed with water, the glass slides were immersed in PDDA solution (1 %) for 20 min and then washed with water again. The PDDA-coated glass slides were then covered with sticky black tapes containing punched holes (9 mm in diameter) to form wells on the surface of the slides. By doing this a fixed area for sample manipulating was defined on all the glass slides, which made the following comparison reasonable. After that, four additional polyelectrolyte layers were assembled on the PDDA-coated glass slides in the sequence of PSS/PAH/PSS/PAH. This is to provide the surface with enough positive charges (the amino group) according to previous reports as well as our own experience. The PSS and PAH solutions were both previously prepared at 2 mgmL−1 in 0.5 M NaCl solution and dissolved by sonication for 15 min. For the deposition of each layer, the polyelectrolyte solution was pipetted into the wells of the slides at 100 μL/well and then incubated for 15 min before being rinsed thoroughly with water. Subsequently, RB was covalently immobilized on the as-prepared polyelectrolyte-coated slides via EDC/NHS crosslinking protocol. Freshly prepared EDC (10 mM, 10 μL) and NHS (0.1 M, 2.5 μL) were added to an RB solution (100 μM, 1 mL) to activate the −COOH groups of RB. After incubated for 15 min at room temperature, the mixture was diluted with PBS to a final concentration of 6 μM in terms of RB molecules, and was then pipetted into the wells of the slides. The activated RB molecules were expected to react with the amine groups of PAH on the slides. After 1 h's reaction in the dark at 37 °C, the slides were rinsed with water and dried under argon. Next, to render the surface protein reactive, a glutaraldehyde solution (5 %) was pipetted into the wells of the slides and allowed to react for 3 h at room temperature. After thoroughly rinsed with water and dried under argon, the fluorescent immune substrates were stored at 4 °C for future use.

Immunoassay Procedures

The model immunoassays were performed in the wells on the fluorescent immune substrates. Human IgG of different concentrations in BBS were added to the wells and incubated overnight at 4 °C in a humid chamber. After washed with TBS-T, TBS and water for three times, blocking was performed with BSA (5 % in BBS) for 3 h at room temperature. After the substrates were rinsed with TBS-T, TBS and water, the previously synthesized SANC were added at 50 μL/well and allowed to react for 2 h in a humid chamber at room temperature. Then the substrates were carefully rinsed with water, dried under argon, and stored at 4 °C until measurement.

Characterization

UV/Vis spectra were measured with a Shimadzu UV-3600 PC spectrophotometer. Aqueous samples were measured in quartz cuvettes of 1 cm path length, using pure water as a control. For samples on glass slides, the slides were placed in a direction such that the incident light beams were perpendicular to the slide surface, and another glass slide covered with black tapes with holes but without samples was used as a control. Fluorescence spectra were measured using an Edinburgh FLS 920 combined fluorescence lifetime and steady-state spectrometer. An excitation of 520 nm from the xenon lamp was used for the measurements, which was incident on the sample surface from the back of the substrate, and from the same side was the emission collected. The power of the excitation at the sample surface and the illuminated sample area were measured to be around 0.17 mW and 7 mm^2, respectively. The integration time was set to 0.5 s. For the measurement of the RB-attached substrates with or without SANC binding, another slide similarly prepared but without RB attachment was used as a background control to eliminate the interference of the background noise.

The size and shape of the nanoparticles were characterized using a transmission electron microscope (Tecnai G^2, Holland). The surface morphology of the SANC-attached substrates were characterized using a scanning electron microscope (S-3000N).

Results and Discussion

Preparation and Characterization of the SANC

The successful conjugation of the GAH IgG to the Ag nanoparticles was confirmed by using two approaches. First, extinction spectra were measured and compared between the raw Ag nanoparticles and the different stages during the synthesis of the SANC, as shown in Fig. 1. The Ag nanoparticles exhibit a strong surface plasmon resonance band
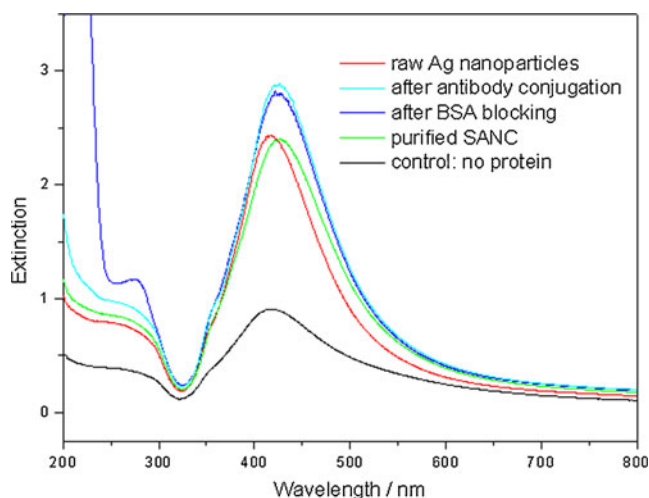
Fig. 1 The extinction spectra at different stages during the synthesis of the SANC. *Red*: raw Ag nanoparticles; *cyan*: after GAH IgG conjugation; *blue*: after BSA blocking; *green*: the SANC after purification. Also shown is a control sample similarly manipulated but without protein incubation (*black*)

with a maximum at around 416 nm. No spectral changes were observed after the pH was adjusted to 9.0 with K_2CO_3. After the incubation with the GAH IgG, the plasmon peak wavelength was red shifted by 9 nm from 416 nm to 425 nm. This is a sign of attachment of the antibodies to the Ag nanoparticles, which is attributed to the increased local refractive index induced by the attached proteins [23]. Blocking the nanoconjugates with BSA does not produce a further red-shifted plasmon peak, which is a necessary step under the stability and specificity considerations. Compared to the raw Ag nanoparticles, the purified SANC are characterized by a similar extinction profile but with a red-shifted plasmon peak wavelength of 425 nm and a slightly broadened linewidth. To further prove the attachment of the proteins, a control experiment was performed following the synthesis procedure of the SANC but without protein addition. After the final centrifugation and redispersion to the original volume, an extinction profile with significantly decreased intensity and broadened
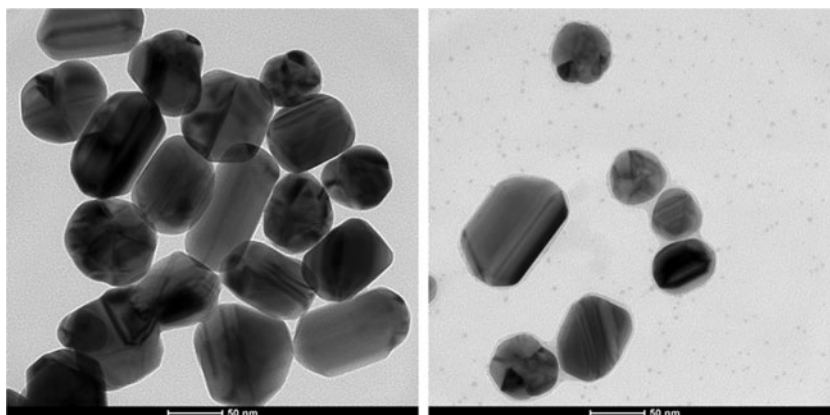
linewidth was observed, indicating the occurrence of a strong aggregation. This is attributed to the relatively weak resistance of Ag nanoparticles to K_2CO_3 in the absence of attached proteins. Second, TEM images of the raw Ag nanoparticles and the SANC were also taken as shown in Fig. 2. The as-prepared raw Ag nanoparticles were heterogeneous in shape, and exhibited a relatively broad size distribution ranging from 50 nm to 120 nm. Importantly, a coating layer around the SANC can be clearly seen compared to the bare surface of the raw Ag nanoparticles, which is consistent with previous reports [24]. Therefore, the successful synthesis of the SANC was confirmed by both UV/Vis spectroscopy and TEM.

Preparation and Characterization of the Fluorescent Immune Substrate

PAH, an amine-enriched polyelectrolyte is employed for the construction of a bifunctional substrate, that is, a substrate with combined fluorescence and protein reactivity. PAH has been used to introduce both of the above-mentioned functions, in which the amino groups play a key role. Parts of the amino groups react with the carboxyl groups of the RB molecules through the well-known EDC/NHS crosslinking protocol, while the rest amino groups react with glutaraldehyde, rendering the surface protein reactive.

Besides the chemical structure with a carboxyl group, RB has been chosen to provide the fluorescence also because of its relatively low quantum yield of less than 0.1, which makes it a good candidate for the SEF experiment. The absorption and the fluorescence spectra of the substrate are characterized by the black line and the red line in Fig. 3a, respectively. To make an estimation of the quantity of RB molecules attached to the substrate, we compare the absorption of the substrate with that of another control slide with a known quantity of RB deposited without any washing procedures. The surface density of RB was estimated to be around 10^{13} cm^{-2}, indicating a relatively small intermolecular distance of RB molecules, which is expected to further reduce the effective quantum yield. Besides, the substrate is protein reactive, which can be

Fig. 2 TEM images of the raw Ag nanoparticles (*left*) and the SANC (*right*)
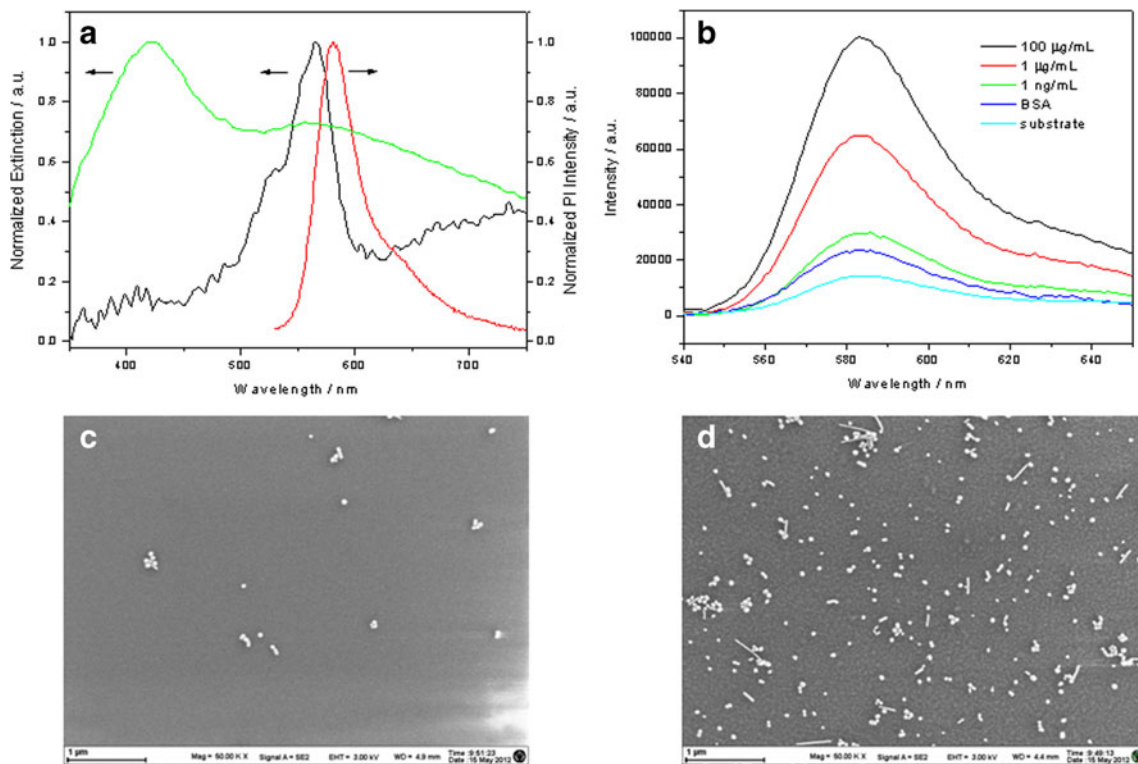
Fig. 3 a The absorption (*black*) and the emission spectra (*red*) of the fluorescent immune substrate. The extinction spectrum of the substrate-immobilized SANC is also shown (*green*). b The fluorescence spectra measured from the fluorescent immune substrate before (*cyan*) and after the SANC incubation at h IgG concentrations of 100 μg/mL

(*black*), 1 μg/mL (*red*) and 1 ng/mL (*green*). The nonspecific fluorescence spectrum is shown by the *blue curve*. c The SEM image of the SANC-attached fluorescent immune substrate with a hIgG concentration of 1 ng/mL. d The SEM image of the SANC-attached fluorescent immune substrate with a hIgG concentration of 1 μg/mL

evidenced by the following immunoassay result with high specificity, as shown in Fig. 3b.

SEF-Based Immunoassay

Prior to the evaluation of the sensing ability, the specificity of the immunoassay scheme was first characterized (shown in Fig. 3b). The cyan line represents the fluorescence of the immune substrate before immunoreaction with the SANC. In the case of 1 μg/mL of IgG immobilization, a significantly enhanced fluorescence was observed as shown by the red line. However, when BSA was used instead of the target hIgG, a much weaker fluorescence was detected, as displayed by the blue line, indicating a relatively good specificity of the immunoassay scheme. It should be noted that the fluorescence signal in this case is higher than that of the substrate alone (the cyan line). This is attributed to the nonspecific adsorption of the SANC onto the BSA immobilized substrate, which is also supported by the extremely weak grey color of the substrate observed after immunoreaction.

The final fluorescence signal varies with varying target antigen concentrations. As more antigens are immobilized on the immune substrate, more SANC are expected to adsorb onto the substrate through the antigen-antibody immunoreaction,

leading to larger fluorescence enhancements of the previously immobilized RB molecules. The black line in Fig. 3b displays the detected fluorescence spectrum for 100 μg/mL of IgG immobilization, which corresponds to an around 7-fold enhancement compared to the original fluorescence before immunoreaction. A less concentration of target IgG leads to a weaker enhancement, as shown by the green line for the case of 1 ng/mL, which is only slightly above the fluorescence level of nonspecific adsorption. One can easily relate the fluorescence enhancement observed in this immunoassay scheme to the surface density of the SANC according to the gray color on the substrate appearing after immunoreaction. SEM images were also taken to address this issue. Figure 3c shows the surface morphology of the SANC-conjugated immune substrate with a hIgG concentration of 1 ng/mL. The SANC were observed as partially aggregated and located sparsely on the substrate surface. In the case of a higher IgG concentration of 1 μg/mL, a higher surface density of the SANC was exhibited, as shown in Fig. 3d. The difference in the surface density of the SANC between immune substrates with different target IgG concentrations clearly indicates the origin of the observed fluorescence enhancement. As previously reported, SEF is a strongly distance-dependent effect and only the dyes within an effective region, generally between 5 and 20 nm from the metal

surface, exhibit an enhanced fluorescence. Consequently, a larger surface density of the nanoparticles corresponds to a larger area of the effective regions, leading to a larger fluorescence enhancement [5].

Recently the exploitation of the detailed mechanism in SEF is receiving special interest. To correlate our enhancement results to the established mechanisms, it would be informative to take a closer look at the extinction characteristics of the SANC on the substrate, which is known to be a key factor in SEF effect. The green line in Fig. 3a depicts the extinction spectrum of the SANC adsorbed on the immune substrate, which deviates from that of the SANC in BBS solution as shown in Fig. 1. The plasmon peak at around 425 nm remains roughly unchanged while a new broad shoulder appears at around 560 nm. This is possibly because of the partial aggregation of the SANC during the process of immunoreaction, which can also be evidenced by the SEM images shown in Fig. 3c and d. Interestingly, the appearance of the shoulder provides an obvious spectral overlap between the extinction of the SANC and the absorption and emission spectra of the attached RB. Such spectral overlaps have been extensively studied and are considered to be important in the SEF effect: An overlap of the extinction of the metallic nanoparticles with the absorption or the emission profile of the dye is expected to result in enhancement in the excitation or the emission process, respectively [25–28]. Moreover, in a comparative experiment, a similar fluorescent immune substrate but with 2-fold less RB

conjugation was prepared. With similar quantities of the SANC attached on the substrate, as monitored from the extinction spectra, only a moderate enhancement of around 2 fold was observed (data not shown). If we assume a homogeneous distribution of the dyes and a similar distribution of the SANC in both cases, the excitation enhancement factors would be approximately the same in both cases. The observed difference in the fluorescence enhancement factors is expected to come from the emission process due to the increased surface density, and thus the decreased effective quantum yield of the RB molecules. Hence, an excitation enhancement of less than 2 fold and an emission enhancement of more than 3.5 fold are estimated in the current experimental format, suggesting a major contribution from the emission process. A precise separation of the excitation and the emission enhancement is of practical importance, as they may find special use separately in different situations. For example, in the design of the solar cells, the absorption enhancement (corresponding to the excitation enhancement in SEF) is highly desired while the emission enhancement is considered to be deleterious [29]. However, in some other cases, such as the plasmon-enhanced LEDs [30, 31] and the chemiluminescence studies [32], the photoexcitation is not involved and only the emission process is considered. A precise separation of the two factors requires more delicately designed experiments [33–35], which is, however, beyond the scope of this manuscript.
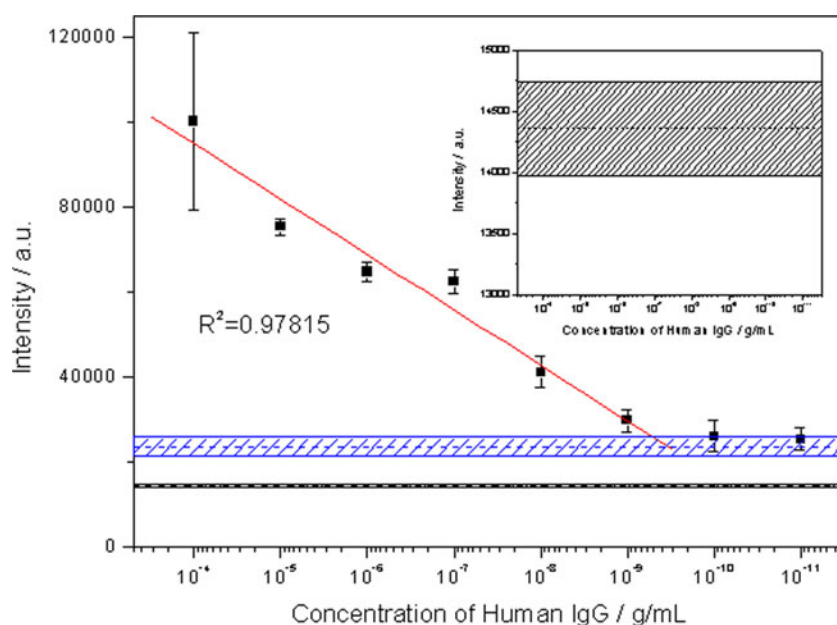
Fig. 4 The calibration curve of the fluorescence signal vs. the concentration of hIgG in the range of 100 μg/mL to 1 ng/mL. The dose-responsive were constructed by averaging three readings of the responses at different locations of each sample. Each *error bar* represents the standard deviation. The linear regression equation is $y=1.306\times 10^4 x+1.472\times 10^5$, and the correlation coefficient (R^2) is 0.97815 ($n=$ 6). The *blue dashed line* and the *blue shaded area* indicate the fluorescence level from the nonspecific SANC adsorption and the corresponding standard deviation, respectively. The *black dashed line* and the *black shaded area* indicate the fluorescence level before the incubation of the SANC and the corresponding standard deviation, respectively. The *inset* shows an enlarged view of this area for clarity

It is necessary to test the dependence of the signal on the target antigen concentration for a given immunoassay format. However, among the various SEF-based immunoassays, only a few have demonstrated the analytical performance and determined the limit of detection (LOD) possibly due to problems such as the inhomogeneous nature of the metallic nanostructures [15, 36]. In our scheme, unlike most previous reports, the metallic nanoparticles are not used as an underlying substrate, but as an exogenous enhancing agent introduced during the immunoassay. The fluorescence output is expected to be directly related to the surface density of the attached SANC. Moreover, the fluorescent immune substrate exhibited a satisfactory repeatability of the original fluorescence, indicated by the relatively small standard deviation shown in Fig. 4 (the black shaded area surrounding the black dashed line, see the inset for clarity). Consequently, exploitation in the analytical performance using the presented scheme seems reasonable. The dependence of the fluorescence intensity on the hIgG concentration was tested and the result was shown in Fig. 4. A linear relationship was exhibited in the range of 100 μg/mL to 1 ng/mL. The linear regression equation was $y=1.306\times 10^4 x+1.472\times 10^5$, and the correlation coefficient (R^2) was 0.97815 ($n=6$). At still lower concentrations, the data points exhibited a different behavior and the fluorescence intensities were difficult to be resolved from the level of the nonspecific binding, as shown by the overlap between the blue shaded area and the last two data points. Thus, the LOD of this immunoassay scheme was deduced to be 1 ng/mL.

Although the obtained 1 ng/mL may not be a very attractive LOD in such immunoassays [15, 36], it should be noted that under the present experimental conditions, a lot of parameters are far from optimum. As can be deduced from Fig. 4, a number of factors can affect the LOD, such as the nonspecific fluorescence level and the fluorescence enhancement factors, especially in the cases of low concentration. A combined higher fluorescence enhancement factor at low concentrations and a lower nonspecific level would lead to an improved LOD in the current immunoassay scheme.

The factors that affect the fluorescence enhancement factor have been extensively studied in various reports and it is of great importance to choose a metal-dye pair properly. Ag nanoparticles are known to be very effective in fluorescence enhancement. However, it is also reported that different kinds of Au nanoparticles can provide greatly enhanced fluorescence in longer wavelength range [37–39]. A spectral overlap between the extinction spectrum of the nanoparticles and the absorption/emission spectra should be attained in the choice of the metal-dye pair [25–28]. Dyes with lower quantum yields have been reported to be more apt to be enhanced compared to the ones with higher quantum yields, which should also be taken into consideration [28]. The metallic nanoparticle size also affects fluorescence enhancement [40, 41]. In our proof-of-concept study, the prepared Ag nanoparticles are heterogeneous in shape, and exhibit a broad size distribution. A better control of the size and shape of the metallic nanoparticles is expected to result in an improved fluorescence enhancement.

Another requirement of achieving a lower LOD is to reduce the nonspecific fluorescence enhancement, which is due to the nonspecific adsorption of the SANC onto the fluorescence immune substrate. The reduction of the nonspecific signal might be achieved by shortening the incubation time. Recently, a novel technique has been introduced which incorporates low power microwave to accelerate the antigen-antibody immunoreaction [42]. By the presumed mechanism of locally heating the proteins in close proximity of the metallic nanostructures, a significantly shortened time for the immunoreaction has been reported without obvious acceleration of the nonspecific adsorption. Incorporating this technique in our immunoassay scheme may lead to the effective reduction of the nonspecific fluorescence level, thus reaching a further lowered LOD. Work is currently under way in this regard.

Conclusions

In this paper, we have introduced a novel SEF-based immunoassay applicable to a wide range of antibodies to eliminate the inconvenience associated with the uses of the dye-labeled antibodies and the metallic nanostructure substrates. A fluorescent immune substrate has been constructed with combined fluorescence and protein reactivity, and used for antigen immobilization. The silver-antibody nanoconjugate has been successfully synthesized and used for specifically recognizing the surface-bound antigens. Upon the specific adsorption of the SANC onto the substrate, an enhanced fluorescence is obtained. With increasing antigen concentrations, the surface density of the SANC is increased, leading to an increased enhancement factor. The dose-responsive performance of the immunoassay scheme has been examined and a LOD of 1 ng/mL is determined. The optimization of the immunoassay scheme has also been discussed. The presented SEF-based immunoassay scheme holds potential in a wide range of bio-applications.

References

1. Gosling JP (1990) A decade of development in immunoassay methodology. Clin Chem 36(8):1408–1427

2. Aslan K, Gryczynski I, Malicka J, Matveeva E, Lakowicz JR, Geddes CD (2005) Metal-enhanced fluorescence: an emerging tool in biotechnology. Curr Opin Biotechnol 16(1):55–62. doi:10.1016/j.copbio.2005.01.001

3. Fort E, Gresillon S (2008) Surface enhanced fluorescence. J Phys D Appl Phys 41(1). doi:10.1088/0022-3727/41/1/013001

4. Li RQ, Xu SH, Wang CL, Shao HB, Xu QY, Cui YP (2010) Metal-enhanced fluorescence of CdTe nanocrystals in aqueous solution. ChemPhysChem 11(12):2582–2588. doi:10.1002/cphc.201000239

5. Zhang RH, Wang ZY, Song CY, Yang J, Li J, Sadaf A, Cui YP (2011) Surface-enhanced fluorescence from fluorophore-assembled monolayers by using Ag@SiO2 nanoparticles. ChemPhysChem 12(5):992–998. doi:10.1002/cphc.201000849

6. Gersten J, Nitzan A (1981) Spectroscopic properties of molecules interacting with small dielectric particles. J Chem Phys 75(3):1139–1152. doi:10.1063/1.442161

7. Ruppin R (1982) Decay of an excited molecule near a small metal sphere. J Chem Phys 76(4):1681–1684. doi:10.1063/1.443196

8. Das PC, Puri A (2002) Energy flow and fluorescence near a small metal particle. Phys Rev B 65(15). doi:10.1103/PhysRevB.65.155416

9. Lakowicz JR (2005) Radiative decay engineering 5: metal-enhanced fluorescence and plasmon emission. Anal Biochem 337(2):171–194. doi:10.1016/j.ab.2004.11.026

10. Ming T, Zhao L, Chen HJ, Woo KC, Wang JF, Lin HQ (2011) Experimental evidence of plasmophores: plasmon-directed polarized emission from gold nanorod-fluorophore hybrid nanostructures. Nano Lett 11(6):2296–2303. doi:10.1021/nl200535y

11. Matveeva EG, Gryczynski Z, Lakowicz JR (2005) Myoglobin immunoassay based on metal particle-enhanced fluorescence. J Immunol Methods 302(1–2):26–35. doi:10.1016/j.jim.2005.04.020

12. Zhang J, Matveeva E, Gryczynski I, Leonenko Z, Lakowicz JR (2005) Metal-enhanced fluoroimmunoassay on a silver film by vapor deposition. J Phys Chem B 109(16):7969–7975. doi:10.1021/jp0456842

13. Shtoyko T, Matveeva EG, Chang IF, Gryczynski Z, Goldys E, Gryczynski I (2008) Enhanced fluorescent immunoassays on silver fractal-like structures. Anal Chem 80(6):1962–1966. doi:10.1021/ac7019915

14. Matveeva EG, Gryczynski I, Barnett A, Leonenko Z, Lakowicz JR, Gryczynski Z (2007) Metal particle-enhanced fluorescent immunoassays on metal mirrors. Anal Biochem 363(2):239–245. doi:10.1016/j.ab.2007.01.030

15. Nooney R, Clifford A, LeGuevel X, Stranik O, McDonagh C, MacCraith BD (2010) Enhancing the analytical performance of immunoassays that employ metal-enhanced fluorescence. Anal Bioanal Chem 396(3):1127–1134. doi:10.1007/s00216-009-3357-9

16. Zhang R, Wang Z, Song C, Yang J, Sadaf A, Cui Y (2012) Immunoassays based on surface-enhanced fluorescence using gap-plasmon-tunable Ag bilayer nanoparticle films. J Fluoresc 1–7. doi:10.1007/s10895-012-1117-2

17. Coons AH, Creech HJ, Jones RN (1941) Immunological properties of an antibody containing a fluorescent group. Proc Soc Exp Biol Med (New York, NY) 47(2):200–202. doi:10.3181/00379727-47-13084p

18. Vira S, Mekhedov E, Humphrey G, Blank PS (2010) Fluorescent-labeled antibodies: balancing functionality and degree of labeling. Anal Biochem 402(2):146–150. doi:10.1016/j.ab.2010.03.036

19. Lee PC, Meisel D (1982) Adsorption and surface-enhanced raman of dyes on silver and gold sols. J Phys Chem 86(17):3391–3395. doi:10.1021/j100214a025

20. Zhang C, Zhang ZY, Yu BB, Shi JJ, Zhang XR (2002) Application of the biological conjugate between antibody and colloid Au nanoparticles as analyte to inductively coupled plasma mass spectrometry. Anal Chem 74(1):96–99. doi:10.1021/ac0103468

21. Chu X, Fu X, Chen K, Shen GL, Yu RQ (2005) An electrochemical stripping metalloimmunoassay based on silver-enhanced gold nanoparticle label. Biosens Bioelectron 20(9):1805–1812. doi:10.1016/j.bios.2004.07.012

22. Ling J, Li YF, Huang CZ (2009) Visual sandwich immunoassay system on the basis of plasmon resonance scattering signals of silver nanoparticles. Anal Chem 81(4):1707–1714. doi:10.1021/ac802152b

23. Mock JJ, Smith DR, Schultz S (2003) Local refractive index dependence of plasmon resonance spectra from individual nanoparticles. Nano Lett 3(4):485–491. doi:10.1021/nl0340475

24. Song W, Mao Z, Liu XJ, Lu Y, Li ZS, Zhao B, Lu LH (2012) Detection of protein deposition within latent fingerprints by surface-enhanced Raman spectroscopy imaging. Nanoscale 4(7):2333–2338. doi:10.1039/c2nr12030e

25. Kuhn S, Hakanson U, Rogobete L, Sandoghdar V (2006) Enhancement of single-molecule fluorescence using a gold nanoparticle as an optical nanoantenna. Phys Rev Lett 97(1). doi:10.1103/PhysRevLett.97.017402

26. Tam F, Goodrich GP, Johnson BR, Halas NJ (2007) Plasmonic enhancement of molecular fluorescence. Nano Lett 7(2):496–501. doi:10.1021/nl062901x

27. Chen Y, Munechika K, Ginger DS (2007) Dependence of fluorescence intensity on the spectral overlap between fluorophores and plasmon resonant single silver nanoparticles. Nano Lett 7(3):690–696. doi:10.1021/nl062795z

28. Munechika K, Chen Y, Tillack AF, Kulkarni AP, Plante IJL, Munro AM, Ginger DS (2010) Spectral control of plasmonic emission enhancement from quantum dots near single silver nanoprisms. Nano Lett 10(7):2598–2603. doi:10.1021/nl101281a

29. Akimov YA, Ostrikov K, Li EP (2009) Surface plasmon enhancement of optical absorption in thin-film silicon solar cells. Plasmonics 4(2):107–113. doi:10.1007/s11468-009-9080-8

30. Okamoto K, Niki I, Shvartser A, Narukawa Y, Mukai T, Scherer A (2004) Surface-plasmon-enhanced light emitters based on InGaN quantum wells. Nat Mater 3(9):601–605. doi:10.1038/nmat1198

31. Kwon MK, Kim JY, Kim BH, Park IK, Cho CY, Byeon CC, Park SJ (2008) Surface-plasmon-enhanced light-emitting diodes. Adv Mater 20(7):1253–1257. doi:10.1002/adma.200701130

32. Aslan K, Geddes CD (2009) Metal-enhanced chemiluminescence: advanced chemiluminescence concepts for the 21st century. Chem Soc Rev 38(9):2556–2564. doi:10.1039/b807498b

33. Chen YC, Munechika K, Jen-La Plante I, Munro AM, Skrabalak SE, Xia YN, Ginger DS (2008) Excitation enhancement of CdSe quantum dots by single metal nanoparticles. Appl Phys Lett 93(5). doi:10.1063/1.2956391

34. Schietinger S, Barth M, Alchele T, Benson O (2009) Plasmon-enhanced single photon emission from a nanoassembled metal-diamond hybrid structure at room temperature. Nano Lett 9(4):1694–1698. doi:10.1021/nl900384c

35. Lang XY, Guan PF, Zhang L, Fujita T, Chen MW (2010) Size dependence of molecular fluorescence enhancement of nanoporous gold. Appl Phys Lett 96(7). doi:10.1063/1.3323104

36. Li H, Qiang WB, Vuki M, Xu DK, Chen HY (2011) Fluorescence enhancement of silver nanoparticle hybrid probes and ultrasensitive detection of IgE. Anal Chem 83(23):8945–8952. doi:10.1021/ac201574s

37. Liu NG, Prall BS, Klimov VI (2006) Hybrid gold/silica/nanocrystal-quantum-dot superstructures: synthesis and analysis of semiconductor–metal interactions. J Am Chem Soc 128(48):15362–15363. doi:10.1021/ja0660296

38. Bardhan R, Grady NK, Cole JR, Joshi A, Halas NJ (2009) Fluorescence enhancement by Au nanostructures: nanoshells and nanorods. ACS Nano 3(3):744–752. doi:10.1021/nn900001q

39. Ming T, Zhao L, Yang Z, Chen HJ, Sun LD, Wang JF, Yan CH (2009) Strong polarization dependence of plasmon-enhanced

fluorescence on single gold nanorods. Nano Lett 9(11):3896–3903. doi:10.1021/nl902095q

40. Nakamura T, Hayashi S (2005) Enhancement of dye fluorescence by gold nanoparticles: analysis of particle size dependence. Jpn J Appl Phys 44(9A):6833–6837. doi:10.1143/jjap.44.6833

41. Zhang J, Fu Y, Chowdhury MH, Lakowicz JR (2008) Single-molecule studies on fluorescently labeled silver particles: effects of particle size. J Phys Chem C 112(1):18–26. doi:10.1021/jp074938r

42. Aslan K, Holley P, Geddes CD (2006) Microwave-Accelerated Metal-Enhanced Fluorescence (MAMEF) with silver colloids in 96-well plates: application to ultra fast and sensitive immunoassays, high throughput screening and drug discovery. J Immunol Methods 312(1–2):137–147. doi:10.1016/j.jim.2006.03.009